

19 low mass hypervelocity star candidates from the first data release of the LAMOST survey

Yin-Bi Li¹, A-Li Luo¹, Gang Zhao¹, You-Jun Lu¹, Peng Wei^{1,2}, Bing Du¹, Xiang Li¹, Yong-Heng Zhao¹, Zhan-Wen Han³, Bo Wang³, Yue Wu¹, Yong Zhang⁴, Yong-Hui Hou⁴, Yue-Fei Wang⁴ and Ming Yang¹

¹ Key Laboratory of Optical Astronomy, National Astronomical Observatories, Chinese Academy of Sciences, Beijing 100012, China; lal@nao.cas.cn; gzhao@bao.ac.cn

² State Key Laboratory of High-end Server & Storage Technology, Jinan 250510, China

³ Key Laboratory for the Structure and Evolution of Celestial Objects, Yunnan Observatories, Chinese Academy of Sciences, Kunming 650216, China

⁴ Nanjing Institute of Astronomical Optics & Technology, National Astronomical Observatories, Chinese Academy of Sciences, Nanjing 210042, China

Received 2015 April 1; accepted 2015 May 20

Abstract Hypervelocity stars are believed to be ejected out from the Galactic center through dynamical interactions between (binary) stars and the central supermassive black hole(s). In this paper, we report 19 low mass F/G/K type hypervelocity star candidates from over one million stars found in the first data release of the LAMOST regular survey. We determine the unbound probability for each candidate using a Monte-Carlo simulation by assuming a non-Gaussian proper-motion error distribution, and Gaussian heliocentric distance and radial velocity error distributions. The simulation results show that all the candidates have unbound possibilities over 50% as expected, and one of them may even exceed escape velocity with over 90% probability. In addition, we compare the metallicities of our candidates with the metallicity distribution functions of the Galactic bulge, disk, halo and globular clusters, and conclude that the Galactic bulge or disk is likely the birth place for our candidates.

Key words: stars: low-mass — stars: kinematics and dynamics — Galaxy: abundances — stars: fundamental parameters — stars: distances

1 INTRODUCTION

Hypervelocity stars (HVSs), discovered in the Galactic halo, are travelling so fast that they can escape from the Galaxy. Hills (1988) first predicted their existence. The actuality of HVSs would provide strong evidence in favor of a supermassive black hole (SMBH) at the center of the Milky Way. A natural explanation is that they may be ejected out from the Galactic center (GC) by interactions between stars and the SMBH or hypothetical binary SMBHs as predicted by Hills (1988) and Yu & Tremaine (2003). Such ejection mechanisms can be divided into three categories: tidal breakup of binary stars in the vicinity of a single SMBH (Hills 1988; Yu & Tremaine 2003; Bromley et al. 2006), in which the binary stars are probably injected into the vicinity of the SMBH from the

young Galactic disk near the GC (e.g., Lu et al. 2010; Zhang et al. 2010) or from the Galactic bulge (Perets 2009a,b); single star encounters with a binary SMBH (Yu & Tremaine 2003; Sesana et al. 2007; Merritt 2006); or single star encounters with a cluster of stellar mass black holes around the SMBH (O’Leary & Loeb 2008).

However, the black hole acceleration mechanism cannot explain a type of HVS such as US 708 (Hirsch et al. 2005), which does not originate from the center of our Galaxy (e.g., Geier et al. 2015). This type of HVS is likely to be the ejected donor remnant of a thermonuclear supernova in the white dwarf + helium star scenario (see Wang & Han 2009; Geier et al. 2015). Researchers are using LAMOST to search for this type of HVS based on the theoretical results of Wang & Han (2009).

Alternatively, other ejection models can also accelerate stars to high speed, for example, the binary disruption of dense stellar clusters in the Galactic disk (Blaauw 1961; Leonard & Dewey 1993; Napiwotzki & Silva 2012). In this case, a supernova explosion of the more massive evolved component can accelerate its companion to high speed. Tidal disruptions of dwarf galaxies in the Milky Way can also produce high velocity stars (Abadi et al. 2009; Lu et al. 2010; Teyssier et al. 2009). Such a mechanism can produce a high speed star stream or a population of old isolated ‘escaped’ (unbound) or ‘wondering’ (bound) stars.

Seventeen years after Hill’s prediction, three HVSs were successively discovered (Brown et al. 2005; Hirsch et al. 2005; Edelmann et al. 2005). They are massive O or B type stars located in the Galactic halo. Until recently, over 20 unbound HVS had been identified (Brown et al. 2009, 2012; Zheng et al. 2014). Most of them are massive B type stars, that are located in the distant Galactic halo with Galactocentric distances larger than 25 kpc. An interesting exception is an identified B type HVS discovered by Zheng et al. (2014), which is the first HVS discovered with the Large Sky Area Multi-Object Fiber Spectroscopic Telescope (LAMOST). It is the brightest HVS currently known, and is located at a Galactocentric distance of 13 kpc.

Assuming a Salpeter initial mass function (IMF), the expected solar mass HVSs are about 10 times more abundant than $3\text{--}4 M_{\odot}$ HVSs (Brown et al. 2009). Kollmeier et al. (2009) systematically searched for such low mass HVSs in about 290 000 spectra from the Sloan Digital Sky Survey (SDSS) (York et al. 2000; Gunn et al. 1998, 2006), however, they found only six metal-poor stars that can be considered as HVS candidates. Li et al. (2012) also searched for F and G type HVSs from over 370 000 stellar spectra from data release seven of the SDSS, and they presented a catalog of low mass metal-poor HVS candidates. Palladino et al. (2014) identified 20 G and K type HVS candidates from approximately 240 000 stars of the Sloan Extension for Galactic Understanding and Exploration (SEGUE) (Yanny et al. 2009). In addition, Zhong et al. (2014) reported a catalog of 28 high velocity star candidates from data release one (DR1) of the LAMOST regular survey (Luo et al. 2015), which covers a much broader color range than ever, and 17 of them are F, G or K type low mass stars. These current searching results might suggest that the IMF of the parent population of these HVSs is top heavy. A top heavy IMF of the HVS parent population is possibly consistent with an origination in the disk (Bartko et al. 2010; Zhang et al. 2013; Kollmeier et al. 2010). In order to distinguish the ejection mechanisms of HVSs and put constraints on the origin of the parent population of HVSs, it is necessary to search for low-mass HVSs.

In this paper, we systematically search for and investigate HVSs with stellar spectra of LAMOST DR1, and find a total of 19 HVS candidates. The structure of this paper is as follows. In Section 2, we introduce LAMOST and DR1 in detail. In Section 3, we present a series of criteria based on spectroscopic, photometric and dynamic properties to select HVS candidates. In Section 4, we analyze the probability that each HVS candidate can escape from our Galaxy. In Section 5, we compare the metallicities of our 19 HVS candidates with the [Fe/H] distributions of the Galactic bulge, disk, halo and associated globular clusters, and conclude that our HVS candidates likely originated from the Galactic bulge or disk. Finally, the discussion and conclusion are given in Section 6.

2 THE FIRST DATA RELEASE OF THE LAMOST REGULAR SURVEY

LAMOST is a 4 meter quasi-meridian reflecting Schmidt telescope. It adopts a novel active optics technique, which allows both a large effective aperture of about 4 m and a wide field of view of 5° . The focal surface of LAMOST has 4000 precisely positioned optical fibers, which are equally distributed among 16 spectrographs. Thus, it can observe 4000 targets simultaneously. Each spectrograph is equipped with a red channel CCD camera and a blue one, which can simultaneously provide red and blue spectra of observed targets respectively (Cui et al. 2012; Wang et al. 1996; Su & Cui 2004; Liu et al. 2015).

The primary scientific goal of the LAMOST survey is to investigate the large-scale structure of the universe, as well as the structure and evolution history of the Galaxy, and it consists of two main parts. The first part is the LAMOST Extra-Galactic Survey (LEGAS) of galaxies, and the second part is the LAMOST Experiment for Galactic Understanding and Exploration (LEGUE) survey of the Milky Way (Zhao et al. 2012; Deng et al. 2012). Considering the science goals and available targets, LEGAS consists of a galaxy survey and a QSO survey, and LEGUE is divided into three parts, i.e., the Galactic Anticenter survey, the disk survey, and the spheroid survey (Liu et al. 2014; Chen et al. 2012; Carlin et al. 2012). The LAMOST Spectroscopic Survey of the Galactic Anticenter (LSS-GAC) covers a significant volume of the Galactic thin/thick disks and halo in a continuous sky area of ~ 3400 square degrees, which is centered on the Galactic Anticenter with Galactic longitudes $150^\circ \leq l \leq 210^\circ$ and latitudes $|b| \leq 30^\circ$ (Liu et al. 2014; Yuan et al. 2015). The disk survey analyzes data from eight bright plates with low latitude along the Galactic plane which are nearly uniformly distributed in the region $0^\circ < \alpha < 67^\circ$ and $42^\circ < \delta < 59^\circ$ (Chen et al. 2012). The halo survey mainly focuses on areas targeted by the SDSS survey, and plans to observe 5.8 million objects with $r < 16.8$ at $|b| > 30^\circ$ (Yang et al. 2012; Deng et al. 2012; Zhang et al. 2012).

After a one year pilot survey (Luo et al. 2012), LAMOST began its first year regular survey from September 2012, and disclosed its DR1 to internal data users and their collaborators in June 2013. DR1 included a total of 2 204 696 wavelength-calibrated and relative flux-calibrated spectra, which consist of 1 944 329 stars, 12 082 galaxies, 5017 quasars and 243 268 unknown objects. These spectra cover a wavelength range of 3690–9100 Å with a resolution of $R \sim 1800$. In addition, DR1 also published five spectroscopic parameter catalogs, which are the regular catalog, the A, F, G and K type stars catalog, the A type stars catalog, the M dwarfs catalog and the observed plate information catalog respectively. The A, F, G and K type stars catalog provides effective temperatures (T_{eff}), surface gravities ($\log g$), metallicities ($[\text{Fe}/\text{H}]$) and heliocentric radial velocities for 1 061 918 stars. These spectroscopic parameters are indispensable for searching and studying HVSs (Luo et al. 2015; Liu et al. 2015).

3 IDENTIFICATION OF THE LAMOST DR1 HVS CANDIDATES

Our HVS candidates are drawn from F, G and K dwarfs in LAMOST DR1. We use five steps to search for them, and the numbers in brackets below indicate the number of stars left after each step.

- (1) Select F, G and K dwarfs from LAMOST DR1 [519 027]. The LAMOST DR1 officially released atmospheric parameters for 1 061 918 A, F, G and K type stars, which are derived by the LAMOST Stellar Parameter Pipeline (LASP) (Luo et al. 2015). We first select F, G and K type stars with $3600 \leq T_{\text{eff}} \leq 7500$, and plot their Hertzsprung-Russell diagram in Figure 1. From Figure 1, we can see that F, G and K dwarfs can be initially selected with the criteria: (1) $\log g > 4.0$, when $3600 \leq T_{\text{eff}} < 6000$; (2) $\log g > 3.75$, when $6000 \leq T_{\text{eff}} \leq 7500$. We totally obtain 737 023 F, G and K type dwarfs. Then, we upload equatorial coordinates of our 737 023 dwarfs to the ‘MyDB’ database of SDSS DR10, and obtain photometry information for 521 618 dwarfs from the ‘PhotoObjall’ table, as well as proper motions of 519 027 dwarfs

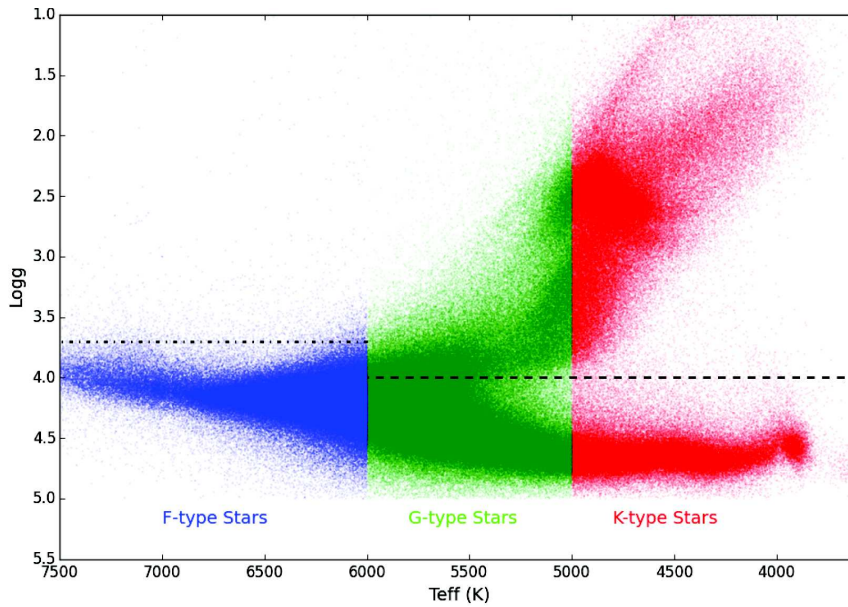


Fig. 1 The Hertzsprung-Russell diagram of F, G and K type stars in LAMOST DR1, where blue, green and red points represent F, G, and K type stars respectively. The black dot-dashed line shows the location of $\log g = 3.75$ for F type stars, and the black dashed line displays $\log g = 4.0$ for G and K type stars.

from the ‘ProperMotions’ table. Finally, 519 027 F, G and K dwarfs with both photometries and proper motions are derived.

(2) Further select F, G and K dwarfs by applying color and magnitude criteria [191 405].

- (a) $g_0 < 20.2$, $r_0 < 19.7$, $0.2 < (g - r)_0 < 0.48$, for F dwarfs
 $r_0 < 19.7$, $0.48 < (g - r)_0 < 0.55$, for G dwarfs
 $r_0 < 19.0$, $0.55 < (g - r)_0 < 0.75$, for K dwarfs
- (b) $A(r) < 0.5$ mag
- (c) $|b| \geq 10$
- (d) $\text{psf Mag Err}_{g/r/i} < 0.05$ mag, mode = 1 and clean = 1
- (e) $0.2 \text{ mag} < (g - i)_0 < 4.0$ mag

Newby et al. (2011) investigated the photometric uncertainties of SDSS, and pointed out that they are constant up to an r -band apparent magnitude (r_0) of 19.7, thus we use criterion (a) listed above to select F, G and K dwarfs. Schlesinger et al. (2012) mentioned that regions above and below the Galactic plane undergo small amounts of extinction. This small amount of reddening can affect target selection, so we use criterion (b) to retain a sample of F, G and K dwarfs with extinction in r -band ($A(r)$) less than 0.5 mag ($A(r) < 0.5$ mag). It is well known that the Schlegel et al. (1998) map has a limited spatial resolution and fails at low Galactic latitudes, and extinction from the Schlegel et al. (1998) map may not represent the true value of targets which may lead to inaccurate distance estimates, thus we use criterion (c) to remove dwarfs with $|b| < 10$. In addition, in order to make sure that SDSS photometry is reliable, we use criterion (d) to constrain SDSS psf mag errors in g , r and i bands lower than 0.05 mag, and the value of photometric flag ‘mode’ and ‘clean’ are 1. In the end, we constrain our sample of dwarfs to the color range $0.2 < (g - i)_0 < 4.0$ mag, which is a reliable range to estimate absolute magnitude with the photometric parallax relation of Ivezić et al. (2008).

- (3) Calculate phase space coordinates and escape velocities [191 405]. We first calculate heliocentric distances for 191 405 F, G and K dwarfs using the distance modulus:

$$d(\text{kpc}) = \frac{10^{0.2 \times (r_0 - M_r)}}{100}, \quad (1)$$

where d is the heliocentric distance in the unit of kpc, r_0 is the r -band dereddened apparent magnitude taken directly from the SDSS DR10 ‘PhotoObjAll’ table, and M_r is the r -band absolute magnitude.

The above step constrains our dwarfs to the color range $0.2 < (g - i)_0 < 4.0$ mag, thus we use the photometric parallax relation proposed by Ivezić et al. (2008) to estimate M_r

$$M_r((g - i)_0, [\text{Fe}/\text{H}]) = M_r^0((g - i)_0) + \Delta M_r([\text{Fe}/\text{H}]), \quad (2)$$

where $M_r^0(g - i)$ is the color-magnitude relation and $\Delta M_r([\text{Fe}/\text{H}])$ is the absolute magnitude correction. These values can be calculated by equations (A7) and (A2) of Ivezić et al. (2008), respectively. The $(g - i)_0$ color is available from the table ‘PhotoObjAll’ of SDSS DR10, and the metallicity abundance $[\text{Fe}/\text{H}]$ can be obtained from the A, F, G and K type stars catalog of LAMOST DR1.

Then, we use a right-handed Cartesian coordinate system with its origin being the Galactic center (GC) to calculate Galactic three dimensional (3D) space positions. The X axis points from the Sun to the GC with the Sun at $x = -8$ kpc, the Y axis points in the direction of rotation and the Z axis points towards the North Galactic Pole. We use a similar coordinate system to calculate Galactic 3D velocity, and assume that the motion of the local standard of rest (LSR) is 220 km s^{-1} , and the velocity of the Sun with respect to the LSR is $(11.1 \text{ km s}^{-1}, 12.24 \text{ km s}^{-1}, 7.25 \text{ km s}^{-1})$ (Schönrich et al. 2010).

To determine which dwarfs are unbound to the Galaxy, we adopt five different Galactic potential models to estimate escape velocities (V_{esc}), i.e., a spherically symmetric convergent model (Xue et al. 2008, hereafter Xue08), a spherically symmetric divergent model (Kenyon et al. 2008, hereafter Kenyon08), two axisymmetric divergent models (Paczynski 1990; Koposov et al. 2010, hereafter Paczynski90 and Koposov10), and a triaxial convergent model (Gnedin et al. 2005, hereafter Gnedin05). Except for the simple model of Kenyon08, the four other potentials are all three-component models that include the bulge, disk and halo. Xue08, Koposov10 and Gnedin05 adopt a spherical bulge (Hernquist 1990), which is different from the Miyamoto-Nagai bulge (Miyamoto & Nagai 1975) of Paczynski90. Paczynski90, Koposov10 and Gnedin05 use the Miyamoto-Nagai disk (Miyamoto & Nagai 1975), while Xue08 adopt an exponential disk. For the halo component, the four three-component models are entirely different (Navarro et al. 1996; Paczynski 1990; Fellhauer et al. 2006). For the convergent Galactic potential model, there exists a true escape velocity, and we use Equation (3) to estimate V_{esc}

$$|V_{\text{esc}}(r)| = \sqrt{2 \times |\Phi(r)|}. \quad (3)$$

However, for the divergent potential, any HVS with finite space velocity would not be able to escape from the Galaxy. We thus define unbound stars as ones which can reach $r \geq 200$ kpc with $v \geq +200 \text{ km s}^{-1}$ as shown in Equation (4) (Kenyon et al. 2008)

$$|V_{\text{esc}}(r)| = \sqrt{2 \times \left(\frac{1}{2} \times 200^2 + \|\Phi(r)\| - \|\Phi(200)\| \right)}. \quad (4)$$

- (4) Find HVS candidates with clean and reliable proper motions [32]. In step 2, we use a series of criteria to make sure that our sample of dwarfs has reliable SDSS photometric parameters, which affect the accuracy of heliocentric distance estimates. In addition, the proper motion distribution

of SDSS tends to exhibit large errors. We thus need to ensure that proper motions of dwarfs in our sample are real rather than the product of large errors.

Munn et al. (2004, 2008) presented an improved proper motion catalog, which matched each SDSS point source to the USNO-B catalog (Monet et al. 2003). The SDSS+USNO-B catalog is 90% complete to $g < 19.7$, and has statistical errors of roughly 3–3.5 mas yr⁻¹ and systematic errors of approximately 0.1 mas yr⁻¹ for each component of proper motion. Munn et al. (2004) also defined a series of criteria to make sure that the proper motions from the SDSS catalog are reliable. These criteria were later revised by Kilic et al. (2006) for their white dwarf samples, and Palladino et al. (2014) used the revised criteria when they searched for G and K type HVS candidates in data from SEGUE. In this paper, we use the criteria to select HVS candidates with ‘clean’ or ‘reliable’ proper motions, and a ‘clean’ proper motion is defined as follows:

- (a) $\text{match}=1$, which represents only having one USNO-B object within a 1'' radius of the SDSS target.
- (b) $\text{sigRA} < 525$ and $\text{sigDEC} < 525$, which means that the proper motion fit must have rms residuals less than 525 mas in both the right ascension (RA) and declination (DEC) directions.
- (c) $\text{nFit} \geq 6$, which indicates that at least six observations (SDSS+USNO-B) have been used to determine the proper motion.
- (d) $\text{dist22} > 7$, which suggests the distance to the nearest neighbor with $g < 22$ must exceed 7''.

and a ‘reliable’ proper motion is defined as follows:

- (a) $\text{match}=1$, $\text{sigRA} < 525$ and $\text{sigDEC} < 525$.
- (b) $\text{nFit} = 6$ and $\text{dist22} < 7$; or, $\text{nFit} = 5$ and $\text{dist22} > 7$.

Kilic et al. (2006) pointed out the contamination rate for a target with a ‘reliable’ proper motion is not larger than 1.5%. Finally, we find a total of 32 HVS candidates which can escape from the Galaxy in at least one Galactic potential model mentioned in step 3; 15 of them have ‘clean’ proper motions and another 17 candidates have ‘reliable’ proper motions.

- (5) Finally, HVS candidates are selected with high quality spectra and reliable atmospheric parameters [19]. After applying the above four steps, 32 HVS candidates are initially selected from a sample of over 190 000 F, G and K dwarfs. We further visually inspect their LAMOST spectra, and find ten ‘clean’ proper motion candidates and nine ‘reliable’ proper motion candidates, which have high quality spectra. Values for their r -band signal-to-noise ratio ‘ SNR_r ’ are listed in Table 1. Lee et al. (2008) describe the SEGUE Stellar Parameter Pipeline (SSPP), which was used to derive the fundamental stellar atmospheric parameters (T_{eff} , $\log g$ and $[\text{Fe}/\text{H}]$) for A, F, G and K type stars using multiple methods. We apply the version of the SSPP used for SDSS DR7 to verify atmospheric parameters for 19 HVS candidates, and conclude that the parameters derived by the SSPP are roughly consistent with those obtained by the LASP.

Here, we finally select 19 HVS candidates. All of them have reliable photometry and stellar atmospheric parameters, with over a 98.5% probability of robust proper motions, high quality spectra and no visual blending. Their fundamental parameters, such as equatorial coordinates, r -band dereddened apparent magnitudes and atmospheric parameters, are shown in Table 1, and their heliocentric distances, Galactocentric distances, Galactic rest frame velocity (hereafter called GRF velocity), and escape velocities obtained by the five Galactic potential models are listed in Table 2.

From Table 1, we can see that the value of $[\text{Fe}/\text{H}]$ errors obtained from the LAMOST parameter catalog seem to be large, even much larger than their true value. Such large errors will effect the estimates of error in distance. From Table 2, we can see that the Galactocentric distance errors are very large, and a fraction of them can reach or exceed 10%. Luo et al. (2015) pointed out that external errors associated with parameters from the LAMOST catalog are larger than the real measurement errors, because they rescaled the external errors using a ratio. They compared parameters from the

Table 1 Fundamental Parameters of 19 HVS Candidates

HVS	Designation	R.A. ^a (deg)	Dec ^a (deg)	r_0^b (mag)	SNR _r ^c (6)	rv_{\odot}^d (km s ⁻¹)	$\mu_{\alpha} \cos(\delta)^e$ (mas yr ⁻¹)	μ_{δ}^e (9)	T_{eff}^f (K)	$\log g^f$ (11)	[Fe/H] ^f (12)	[Mg/Fe] ^g (13)
(1)	(2)	(3)	(4)	(5)	(6)	(7)	(8)	(9)	(10)	(11)	(12)	(13)
1	J172524.12+565709.6	261.3505	56.95267	13.95	101	-103±11	-17.19±2.62	88.11±2.62	5251±102	4.65±0.43	-0.76±0.36	0.43
2	J170333.23+373102.3	255.8885	37.51733	17.50	29	-60±10	-22.60±3.00	18.79±3.00	5069±156	4.40±0.41	0.08±0.38	-0.05
3	J132422.30+312841.6	201.0929	31.47823	15.76	18	-23±16	-24.35±2.36	-27.53±2.36	5828±330	4.03±0.66	0.02±0.62	0.33
4	J091255.48+140413.8	138.2312	14.07052	15.26	13	46±22	9.82±2.52	-54.49±2.52	6231±307	4.67±0.36	-0.86±0.82	0.57
5	J130548.65+282410.7	196.4527	28.40298	17.43	16	114±12	-21.49±2.81	-37.11±2.81	5931±447	4.28±0.93	-1.61±1.536	1.11
6	J133115.50+150438.9	202.8146	15.07748	18.49	62	-29±6	-20.87±3.05	4.08±3.05	4854±90	4.68±0.29	0.12±0.24	-0.03
7	J175513.55+511927.4	268.8065	51.3243	13.87	38	-72±11	8.06±2.73	48.98±2.73	5228±170	4.45±0.47	-0.34±0.46	0.32
8	J113116.03+571131.1	172.8168	57.19199	16.19	23	-91±11	-43.52±2.64	-38.49±2.64	6083±259	4.07±0.50	-1.47±0.89	0.58
9	J121811.06+284659.9	184.5461	28.78333	14.08	54	-18±8	-48.94±2.57	-0.32±2.57	5068±117	4.64±0.35	0.04±0.30	-0.03
10	J115209.12+120258.0	178.038	12.04946	15.86	22	206±15	-32.11±2.51	19.24±2.51	5669±280	4.11±0.64	-0.01±0.57	0.10
11	J004028.68+393853.0	10.11953	39.64808	16.13	19	-54±23	-34.08±2.57	-23.19±2.57	6119±290	4.31±0.50	-0.51±0.69	0.42
12	J171952.43+525035.6	259.9685	52.84325	15.62	24	-67±13	-32.84±3.2	83.20±3.2	5703±244	4.20±0.59	-0.11±0.51	0.27
13	J063934.38+280912.8	99.89327	28.15358	17.02	8	15±30	0.11±2.52	15.04±2.52	6064±431	3.94±0.59	-0.33±0.88	-0.18
14	J005233.53+413322.6	13.13972	41.5563	14.81	23	-30±23	-48.83±2.55	-32.97±2.55	6187±282	4.34±0.48	-0.43±0.64	0.02
15	J012947.93-021343.2	22.44971	-2.228684	14.85	50	13±13	-24.22±3.82	30.44±3.82	5860±183	4.25±0.56	-0.36±0.42	0.26
16	J075303.30+272657.0	118.2638	27.44918	17.81	14	75±32	-18.13±3.00	4.51±3.00	6017±399	4.26±0.70	-0.39±0.75	0.36
17	J142235.20+455631.3	215.6467	45.94204	14.89	44	-121±12	-42.77±2.43	11.14±2.43	5231±138	4.68±0.43	-0.57±0.44	0.38
18	J130744.34-004449.5	196.9348	-0.747102	17.18	9	14±20	-9.72±3.11	11.48±3.11	6035±408	4.28±0.50	-0.27±0.86	0.56
19	J103858.44+565558.1	159.7435	56.93283	13.74	74	-15±14	-88.10±5.61	97.36±5.61	5785±146	4.28±0.54	-0.74±0.41	0.36

Notes. The candidates HVS1—HVS10 have ‘clean’ proper motions, and the candidates HVS11—HVS19 have ‘reliable’ proper motions.

^a Equatorial coordinate from the SDSS ‘PhotoObjAll’ catalog.

^b Dereddened r band apparent magnitude from the SDSS ‘PhotoObjAll’ catalog.

^c r -band signal to noise ratio from the LAMOST parameter catalog.

^d Heliocentric radial velocity from the LAMOST parameter catalog.

^e Proper motion in both RA and DEC directions from the SDSS ‘ProperMotions’ catalog.

^f Atmospheric parameters from the LAMOST parameter catalog.

^g Note that there are large uncertainties in [Mg/Fe] measurements.

Table 2 Kinematic Parameters of 19 HVS Candidates

HVS	d_{\odot}^a (kpc)	R_G^b (kpc)	V_G^c (km s ⁻¹)	$V_{\text{esc}}-\text{Xue}^d$ (km s ⁻¹)	$V_{\text{esc}}-\text{Paczynski}^d$ (km s ⁻¹)	$V_{\text{esc}}-\text{Koposv}^d$ (km s ⁻¹)	$V_{\text{esc}}-\text{Kenyon}^d$ (km s ⁻¹)	$V_{\text{esc}}-\text{Gnedin}^d$ (km s ⁻¹)
1	1.5±0.2	8.0±0.2(0.1)	644±96	491	540	573	592	607
2	4.6±0.9	7.5±0.9(0.3)	626±98	500	540	572	603	608
3	4.6±1.5	9.0±1.5(0.5)	572±195	493	523	555	595	596
4	2.9±0.9	10.1±0.9(0.3)	563±178	474	519	551	574	590
5	3.7±1.4	8.7±1.4(0.4)	540±218	492	527	559	593	599
6	5.9±0.8	8.7±0.8(0.5)	524±101	505	524	555	608	598
7	1.9±0.4	7.9±0.4(0.2)	503±83	492	541	575	594	608
8	2.5±0.6	9.4±0.6(0.3)	501±119	481	524	557	581	595
9	2.5±0.5	8.7±0.5(0.3)	490±98	488	530	562	589	600
10	2.3±0.7	8.5±0.7(0.3)	489±92	489	532	565	590	602
11	3.0±0.9	9.8±0.9(0.2)	671±115	476	523	556	576	593
12	1.4±0.4	7.9±0.4(0.1)	621±138	492	541	575	593	608
13	5.5±2.3	13.5±2.3(0.7)	613±157	451	496	527	548	569
14	1.8±0.5	9.0±0.5(0.2)	603±91	482	530	564	582	599
15	2.0±0.4	8.9±0.4(0.2)	591±60	484	529	562	585	599
16	5.1±1.7	12.7±1.7(0.4)	583±104	457	499	530	554	573
17	3.1±0.6	8.5±0.6(0.3)	561±93	491	531	563	592	601
18	6.1±2.6	8.4±2.6(0.8)	527±140	506	526	557	609	600
19	0.6±0.1	8.3±0.1(0.04)	508±42	488	538	572	589	605

^a Heliocentric distances obtained by the distance modulus.

^b Galactocentric distances.

^c GRF velocities.

^d Escape velocities obtained by the Xue08, Paczynski90, Koposov10, Kenyon08 and Gnedin05 Galactic potential models.

LASP with results from high resolution spectra, from SDSS DR9, and Gao et al. (2015, in preparation) and the LAMOST Stellar Parameter Pipeline at Peking University (LSP3) (Xiang et al. 2015). The mean external error is 0.125 dex which is much closer to the true error. Considering this mean error to be [Fe/H] errors in our 19 candidates, the corresponding errors in Galactocentric distance are listed in parentheses in the third column of Table 2. They are much smaller.

Theoretically, Ivezić et al. (2008) pointed out that a 1.0 dex [Fe/H] error will lead to a 1 mag error in absolute magnitude (M_r) at the median thin-disk metallicity ([Fe/H] = -0.2), and a 0.57 mag M_r error at the median halo metallicity ([Fe/H] = -1.50), which demonstrates the mean LAMOST external [Fe/H] error of 0.125 dex will result in an M_r error of 0.125 mag at most, and an error in Galactocentric distance of approximately 6%.

In addition, we check whether our candidates are new findings. Kollmeier et al. (2009) present six F/G type metal-poor HVS candidates from over 290 000 SDSS stars. Li et al. (2012) proposed 13 F and G type metal-poor unbound HVS candidates from SDSS DR7, and Palladino et al. (2014) found 20 G and K type unbound HVS candidates in SEGUE G and K dwarf samples from SDSS DR9. By cross-matching with equatorial coordinates, we find our 19 HVS candidates are not in the three HVS catalogs. Moreover, Zhong et al. (2014) presented a catalog of 28 high-velocity star candidates from LAMOST DR1. They use velocity criteria $|rv| > 200 \text{ km s}^{-1}$ and $|V_{\text{gt}}| \geq 300 \text{ km s}^{-1}$ when selecting HVS candidates, where rv is the heliocentric radial velocity and V_{gt} is the 3D velocity. These criteria prevent all our candidates except for one from being found. Because the exceptional candidate is not in the $u - g$ and $r - i$ color ranges where Zhong et al. (2014) estimate accurate photometric metallicity, it is also included in our catalog of HVS candidates. Among their 28 HVS samples, there are 12 stars with spectral type earlier than F type, and another 16 candidates are eliminated by our photometry and proper motion criteria. In summary, we can conclude that our 19 low mass F/G/K type HVS candidates are new findings.

4 ESTIMATING THE RELIABILITY OF OUR CANDIDATES WITH A MONTE CARLO METHOD

Although we use a series of criteria to ensure our HVS candidates have reliable photometry, atmospheric parameters and proper motions as described in Section 3, it is still premature to say that the final sample of HVS does not contain false-positive detections. With this in mind, we thus consider the probability that our HVS candidates are in fact unbound to the Milky Way. To obtain such an unbound probability for each HVS in our sample, we construct a Monte Carlo simulation to sample a million realizations of orbital parameters.

Dong et al. (2011) present a non-Gaussian probability density function (PDF) of proper motion errors using quasar samples with ‘clean’ proper motions, which contains a Gaussian core and an extended wing. Applying this error distribution model, we randomly produce a million total proper motion errors (pm_{error}) with the inverse function method. Assuming the proper motion error is isotropic in the RA-DEC plane, we can produce a million angles ‘ θ ’ using a uniform distribution model, and obtain a million proper motion errors in the RA and DEC directions using $\text{pmra}_{\text{error}} = \text{pm}_{\text{error}} \times \cos(\theta)$ and $\text{pmdec}_{\text{error}} = \text{pm}_{\text{error}} \times \sin(\theta)$, where $\text{pmra}_{\text{error}}$ and $\text{pmdec}_{\text{error}}$ are random proper motion errors in the RA and DEC directions respectively. Using the proper motion measurements from SDSS in the RA and DEC directions, two component proper motion errors from SDSS and the random proper motion errors $\text{pmra}_{\text{error}}$ and $\text{pmdec}_{\text{error}}$, we can obtain a million random two component proper motions.

In addition, we randomly generate a million radial velocities and heliocentric distances assuming a Gaussian error distribution function. A million random Galactic 6D phase space coordinates and escape velocities at each Galactocentric distance in the million realizations can be further obtained. In such a Monte Carlo simulation, the unbound probability for each HVS candidate can be derived

Table 3 Probabilities that these Candidates are Unbound in Five Galactic Potential Models

HVS	$P_{\text{unbound-Xue08}}^a$	$P_{\text{unbound-Paczynski90}}^a$	$P_{\text{unbound-Koposov10}}^a$	$P_{\text{unbound-Kenyon08}}^a$	$P_{\text{unbound-Gnedin05}}^a$
1	0.93	0.84	0.75	0.86	0.64
2	0.80	0.72	0.64	0.70	0.54
11	0.87	0.80	0.75	0.82	0.67
12	0.80	0.70	0.62	0.71	0.53
13	0.81	0.73	0.67	0.75	0.58
14	0.80	0.69	0.60	0.71	0.51
16	0.77	0.68	0.61	0.70	0.51
15	0.89	0.75	0.62	0.77	— ^b
3	0.61	0.57	0.52	—	—
4	0.64	0.57	0.52	—	—
5	0.57	0.52	—	—	—
6	0.58	0.52	—	—	—
17	0.69	0.58	—	—	—
18	0.53	0.50	—	—	—
7	0.54	—	—	—	—
8	0.54	—	—	—	—
9	0.51	—	—	—	—
10	0.50	—	—	—	—
19	0.63	—	—	—	—

^a Unbound probability obtained by the Xue08, Paczynski90, Koposov10, Kenyon08 and Gnedin05 potential models.

^b ‘—’ means the candidate is bound in a certain potential model, and we do not calculate unbound probability in this case.

by the fraction $\frac{N_{V_{\text{gt}} > V_{\text{esc}}}}{1000000}$, where V_{gt} and V_{esc} are the GRF velocity and Galactic escape velocities respectively, and $N_{V_{\text{gt}} > V_{\text{esc}}}$ is the number of V_{gt} larger than V_{esc} in a million realizations.

Table 3 lists unbound probabilities for each HVS candidate, and ‘—’ in this table indicates that the candidate is bound (meaning not unbound) in this potential model, and we do not calculate unbound probabilities in these cases. From this table, we can see that the unbound probability for each HVS candidate exceeds 0.5 as expected, and it is even over 0.9 for HVS1 in the Xue08 potential model. In addition, for each HVS candidate, the value of unbound probability depends on the adopted Galaxy potential model to a certain extent, such as HVS1. The probability varies from 0.64 in the Gnedin05 model to 0.93 in the Xue08 model, and the difference in probability between the two potential models changes from 0.07 to 0.29. Among our sample of 19 HVSSs, only seven candidates are unbound in all five potential models.

Figure 2 shows their distribution of $V_{\text{gal}} - V_{\text{esc}}$, where V_{gal} and V_{esc} are the GRF velocity and escape velocities for each realization respectively. From this figure, we can see that the total velocity exceeds escape velocity in most cases.

Actually, the value of unbound probability mainly depends on the difference between the GRF velocity and escape velocity. When the total velocity is much larger than the escape velocity, the effect of parameter error and Galactic potential model will be extremely small. Conversely, when total velocity is just larger than the escape velocity, errors in the parameters and which potential model is used greatly affect the unbound probability. In addition, the unbound probability from such a Monte Carlo simulation can only represent the probability of being unbound from the Galaxy when kinematic parameters are in given error ranges.

5 METALLICITY DISTRIBUTION AND POSSIBLE ORIGINS

Investigation of the metallicity distribution of Galactic populations, including the Galactic bulge, the Galactic disk, the Galactic halo and associated globular clusters, indicate each population has a significantly different metal abundance distribution compared to the others. Moreover, metallicity abundance ([Fe/H]) for a star is indicative of the place where it was born. So, the metallicity distribution can be used as a tool to explore the origin of our HVS candidates.

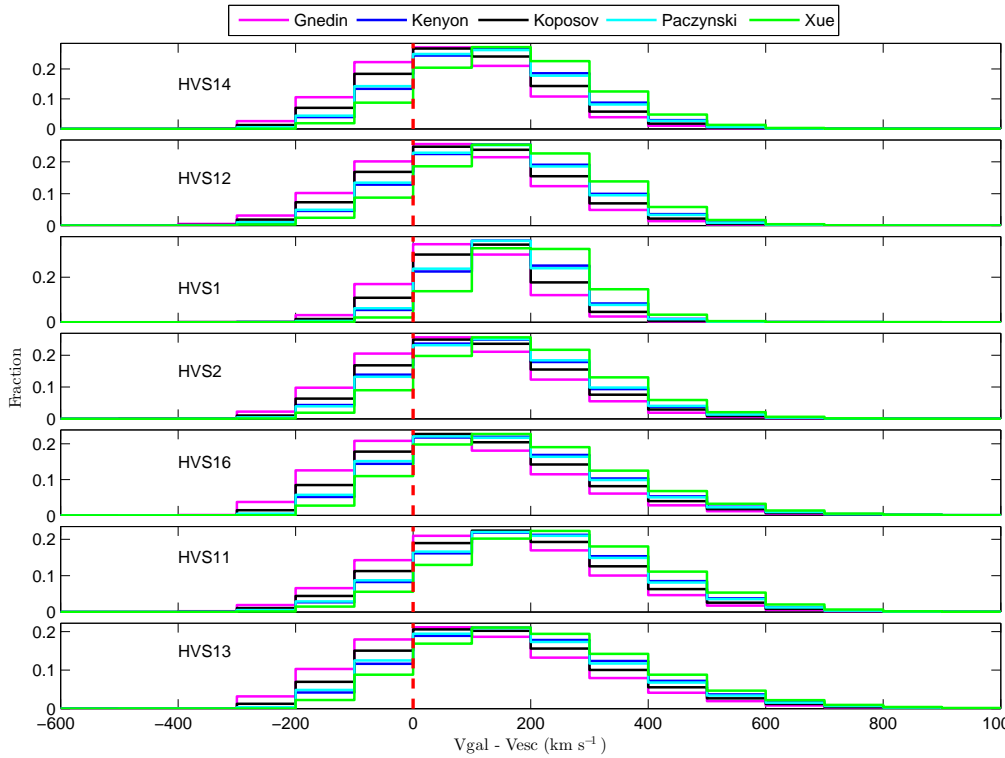


Fig. 2 The distribution of the difference between V_{gal} and V_{esc} , where V_{gal} and V_{esc} are respectively the GRF velocities and escape velocities of each sample realization for a million random samples from the Monte Carlo simulation.

Sadler et al. (1996) measured $[\text{Fe}/\text{H}]$ for 322 K giants in the Galactic bulge, and present the metallicity distribution function (MDF) for the Galactic bulge. They found that the mean abundance of their sample of K giants is $\langle [\text{Fe}/\text{H}] \rangle = -0.11 \pm 0.03$, and over half of them are in the range $-0.4 < [\text{Fe}/\text{H}] < 0.3$. Schlesinger et al. (2012) derived the MDF of the Galactic disk using 24 270 G and 16 847 K dwarfs from SDSS/SEGUE. Different from previous investigations, this work considered observational biases for the first time, and their samples of G and K dwarfs are the most complete samples in both number and volume. An et al. (2013) estimated metal abundance for individual stars in SDSS Stripe 82, and presented an unbiased MDF of the Galactic halo. Harris (1997) compiled a catalog which contains basic parameters of distances, velocities, metallicities, luminosities, colors and dynamical parameters for 147 globular clusters in the Milky Way. We obtained their catalog from the website <http://vizier.china-vo.org/viz-bin/VizieR?-source=VII/202&ref=VIZ55014f467633>.

We compare the metallicities of our candidates with the MDFs of the Galactic bulge (Sadler et al. 1996), the Galactic disk (Schlesinger et al. 2012), the Galactic halo (An et al. 2013) and known globular clusters (Harris 1997). The MDFs for each Galactic population and our candidates are shown in Figure 3. From this figure, we can see that the metallicity distribution of our HVS candidates is very consistent with the sample of G and K dwarfs in the disk, and is also roughly consistent with the low-metallicity end of the Galactic bulge. However, the MDF of our candidates is completely inconsistent with that of the Galactic halo and globular clusters.

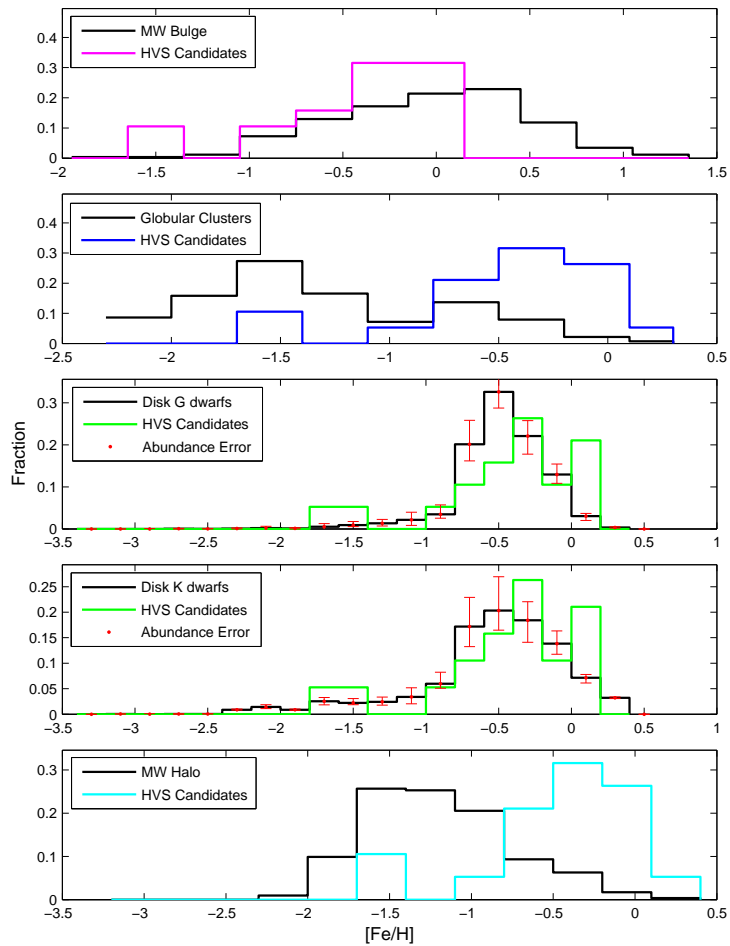


Fig. 3 The comparison of metallicity distribution for 19 HVS candidates with the Galactic bulge, disk, halo and globular clusters.

In addition, we estimate Mg abundances $[Mg/Fe]$ using a profile matching method in the region of Mg I b lines around $\lambda 5170 \text{ \AA}$ (Li et al. 2014), and they are listed in the last column of Table 1. The external uncertainty of this profile matching method may not be as large as 0.2 dex, and the upper limit of internal uncertainty is 0.3 dex, as estimated by the Monte Carlo simulation. From Table 1, we can see that the Mg abundances of four candidates, i.e. HVS4, HVS5, HVS8 and HVS18, are larger than 0.5. We visually inspect the spectra of the four candidates, and find that the noise seriously affects spectral quality of the Mg I b region which is extremely important for the estimation of $[Mg/Fe]$. So, we do not regard the four candidates as Mg-enhanced stars. For other candidates, they have high quality spectra in the Mg I b region, and their $[Mg/Fe]$ values fall within the range of error. Similarly, the $[Mg/Fe]$ values of our candidates are roughly consistent with the Galactic bulge and disk.

Therefore, our candidates likely originated from the Galactic bulge or disk, and the Galactic halo and globular clusters are probably not their place of origin. However, the determination of a more specific birth place needs much more reliable parameters, which will be made public in a future data

release of LAMOST. This can be used to calculate the intersection regions between our candidates' trajectories and the Galactic disk.

6 DISCUSSION AND CONCLUSIONS

In this paper, we present 19 F, G or K type HVS candidates from over one million stars that are part of the LAMOST DR1. We initially select over half a million F, G and K dwarfs with T_{eff} and $\log g$ criteria, and then further pick out over 190 000 final F, G and K dwarfs to make a sample using a series of photometric criteria. Then, we obtain 6D phase space coordinates and escape velocities for each dwarf, and select 17 HVS candidates with 'clean' proper motions and 15 candidates with 'reliable' proper motions. We finally individually inspect spectra from the 32 HVS candidates, and find 19 of them have high quality spectra. Through checking with four previous low mass HVS catalogs in literatures, we conclude that they are all new findings.

Although we use strict criteria to ensure reliability of the kinematic parameters from our candidates, we still cannot confirm that we identify 19 HVS. Therefore, we calculate the unbound probability for each candidate using a Monte Carlo simulation, assuming a non-Gaussian proper motion error distribution and Gaussian heliocentric distance and radial velocity error distributions. Such a probability shows that each of our candidates could escape from the Milky Way. We find all the candidates have unbound probabilities over 50%. One of them can even exceed escape velocity with over 90% probability, and the unbound probability varies in different potential models for each candidate. To investigate the origin of our candidates, we compare metallicities of our candidates with MDFs of the Galactic bulge, disk, halo and associated globular clusters, and conclude that the Galactic bulge or disk is likely the birth place of our candidates, and the Galactic halo or globular clusters are probably not their places of origin.

When we select HVS candidates, there are a large amount of stars with $\text{dist}22 < 7$, which implies that they suffer from photometry blending from their local neighborhood. There are also a large fraction of stars with $\text{nFit} < 5$, which means that they have few position detections. The *Hubble Space Telescope* (HST) Fine Guidance Sensor (FGS) and future *Gaia* mission can provide more accurate proper motion measurements and confirm HVS from them. They can also help us to verify proper motions for our 19 HVS candidates. In addition, high resolution spectroscopic observations are essential for obtaining more accurate measurements of stellar atmospheric parameters, which may help us to determine more accurate places of origin through calculating trajectories and a detailed metallicity distribution analysis, and can also decide whether our HVS candidates are in binaries.

If candidates exist as binaries, their heliocentric distances and Galactic total velocities will be systematically underestimated, and their escape velocities will be correspondingly overestimated. Thus these binaries should be more likely to be able to escape from our Galaxy. Moreover, we estimated the effect of binary orbital velocities on the observed heliocentric radial velocities and the Galactic total velocities assuming three types of companions (e.g., a solar mass main sequence companion, a neutron star companion and a black hole companion) in our previous work (Li et al. 2012), and we can see that the average effect of binaries does not exceed 100 km s^{-1} , which has little effect on our results.

Acknowledgements We thank an anonymous referee for very useful comments that improved the presentation of the paper. We thank Lauren E. Palladino for a valuable discussion of proper motion in a random sample when conducting an unbound probability simulation. This work is supported by the National Natural Science Foundation of China (Grant Nos. 11303036, 11390371/4 and 11233004). The Guo Shou Jing Telescope (the Large Sky Area Multi-Object Fiber Spectroscopic Telescope, LAMOST) is a National Major Scientific Project built by the Chinese Academy of Sciences. Funding for the project has been provided by the National Development and Reform Commission. LAMOST is operated and managed by National Astronomical Observatories, Chinese Academy of Sciences. The web site of LAMOST DR1 is <http://dr1.lamost.org>.

References

- Abadi, M. G., Navarro, J. F., & Steinmetz, M. 2009, *ApJ*, 691, L63
- An, D., Beers, T. C., Johnson, J. A., et al. 2013, *ApJ*, 763, 65
- Bartko, H., Martins, F., Trippe, S., et al. 2010, *ApJ*, 708, 834
- Blaauw, A. 1961, *Bull. Astron. Inst. Netherlands*, 15, 265
- Bromley, B. C., Kenyon, S. J., Geller, M. J., et al. 2006, *ApJ*, 653, 1194
- Brown, W. R., Geller, M. J., Kenyon, S. J., & Kurtz, M. J. 2005, *ApJ*, 622, L33
- Brown, W. R., Geller, M. J., & Kenyon, S. J. 2009, *ApJ*, 690, 1639
- Brown, W. R., Geller, M. J., & Kenyon, S. J. 2012, *ApJ*, 751, 55
- Carlin, J. L., Lépine, S., Newberg, H. J., et al. 2012, *RAA (Research in Astronomy and Astrophysics)*, 12, 755
- Chen, L., Hou, J.-L., Yu, J.-C., et al. 2012, *RAA (Research in Astronomy and Astrophysics)*, 12, 805
- Cui, X.-Q., Zhao, Y.-H., Chu, Y.-Q., et al. 2012, *RAA (Research in Astronomy and Astrophysics)*, 12, 1197
- Deng, L.-C., Newberg, H. J., Liu, C., et al. 2012, *RAA (Research in Astronomy and Astrophysics)*, 12, 735
- Dong, R., Gunn, J., Knapp, G., Rockosi, C., & Blanton, M. 2011, *AJ*, 142, 116
- Edelmann, H., Napiwotzki, R., Heber, U., Christlieb, N., & Reimers, D. 2005, *ApJ*, 634, L181
- Fellhauer, M., Belokurov, V., Evans, N. W., et al. 2006, *ApJ*, 651, 167
- Geier, S., Fürst, F., Ziegerer, E., et al. 2015, *Science*, 347, 1126
- Gnedin, O. Y., Gould, A., Miralda-Escudé, J., & Zentner, A. R. 2005, *ApJ*, 634, 344
- Gunn, J. E., Carr, M., Rockosi, C., et al. 1998, *AJ*, 116, 3040
- Gunn, J. E., Siegmund, W. A., Mannery, E. J., et al. 2006, *AJ*, 131, 2332
- Harris, W. E. 1997, *VizieR Online Data Catalog*, 7202, 0
- Hernquist, L. 1990, *ApJ*, 356, 359
- Hills, J. G. 1988, *Nature*, 331, 687
- Hirsch, H. A., Heber, U., O'Toole, S. J., & Bresolin, F. 2005, *A&A*, 444, L61
- Ivezić, Ž., Sesar, B., Jurić, M., et al. 2008, *ApJ*, 684, 287
- Kenyon, S. J., Bromley, B. C., Geller, M. J., & Brown, W. R. 2008, *ApJ*, 680, 312
- Kilic, M., Munn, J. A., Harris, H. C., et al. 2006, *AJ*, 131, 582
- Kollmeier, J. A., Gould, A., Knapp, G., & Beers, T. C. 2009, *ApJ*, 697, 1543
- Kollmeier, J. A., Gould, A., Rockosi, C., et al. 2010, *ApJ*, 723, 812
- Koposov, S. E., Rix, H.-W., & Hogg, D. W. 2010, *ApJ*, 712, 260
- Lee, Y. S., Beers, T. C., Sivarani, T., et al. 2008, *AJ*, 136, 2022
- Leonard, P. J. T., & Dewey, R. J. 1993, in *Astronomical Society of the Pacific Conference Series*, 45, *Luminous High-Latitude Stars*, ed. D. D. Sasselov, 239
- Li, Y., Luo, A., Zhao, G., et al. 2012, *ApJ*, 744, L24
- Li, X., Zhao, G., Chen, Y.-Q., & Li, H.-N. 2014, *RAA (Research in Astronomy and Astrophysics)*, 14, 1423
- Liu, X.-W., Yuan, H.-B., Huo, Z.-Y., et al. 2014, in *IAU Symposium*, 298, eds. S. Feltzing, G. Zhao, N. A. Walton, & P. Whitelock, 310
- Liu, X. W., Zhao, G., & Hou, J. L. 2015, *RAA (Research in Astronomy and Astrophysics)*, 15, 1089
- Lu, Y., Zhang, F., & Yu, Q. 2010, *ApJ*, 709, 1356
- Luo, A.-L., Zhang, H.-T., Zhao, Y.-H., et al. 2012, *RAA (Research in Astronomy and Astrophysics)*, 12, 1243
- Luo, A. L., Zhao, Y. H., Zhao, G., et al. 2015, *RAA (Research in Astronomy and Astrophysics)*, 15, 1095
- Merritt, D. 2006, *ApJ*, 648, 976
- Miyamoto, M., & Nagai, R. 1975, *PASJ*, 27, 533
- Monet, D. G., Levine, S. E., Canzian, B., et al. 2003, *AJ*, 125, 984
- Munn, J. A., Monet, D. G., Levine, S. E., et al. 2004, *AJ*, 127, 3034
- Munn, J. A., Monet, D. G., Levine, S. E., et al. 2008, *AJ*, 136, 895
- Napiwotzki, R., & Silva, M. D. V. 2012, *Mem. Soc. Astron. Italiana*, 83, 272

- Navarro, J. F., Frenk, C. S., & White, S. D. M. 1996, *ApJ*, 462, 563
- Newby, M., Newberg, H. J., Simones, J., Cole, N., & Monaco, M. 2011, *ApJ*, 743, 187
- O'Leary, R. M., & Loeb, A. 2008, *MNRAS*, 383, 86
- Paczynski, B. 1990, *ApJ*, 348, 485
- Palladino, L. E., Schlesinger, K. J., Holley-Bockelmann, K., et al. 2014, *ApJ*, 780, 7
- Perets, H. B. 2009a, *ApJ*, 690, 795
- Perets, H. B. 2009b, *ApJ*, 698, 1330
- Sadler, E. M., Rich, R. M., & Terndrup, D. M. 1996, *AJ*, 112, 171
- Schlegel, D. J., Finkbeiner, D. P., & Davis, M. 1998, *ApJ*, 500, 525
- Schlesinger, K. J., Johnson, J. A., Rockosi, C. M., et al. 2012, *ApJ*, 761, 160
- Schönrich, R., Binney, J., & Dehnen, W. 2010, *MNRAS*, 403, 1829
- Sesana, A., Haardt, F., & Madau, P. 2007, *MNRAS*, 379, L45
- Su, D.-Q., & Cui, X.-Q. 2004, *ChJAA (Chin. J. Astron. Astrophys.)*, 4, 1
- Teysier, M., Johnston, K. V., & Shara, M. M. 2009, *ApJ*, 707, L22
- Wang, S.-G., Su, D.-Q., Chu, Y.-Q., Cui, X., & Wang, Y.-N. 1996, *Appl. Opt.*, 35, 5155
- Wang, B., & Han, Z. 2009, *A&A*, 508, L27
- Xiang, M. S., Liu, X. W., Yuan, H. B., et al. 2015, *MNRAS*, 448, 822
- Xue, X. X., Rix, H. W., Zhao, G., et al. 2008, *ApJ*, 684, 1143
- Yang, F., Carlin, J. L., Liu, C., et al. 2012, *RAA (Research in Astronomy and Astrophysics)*, 12, 781
- Yanny, B., Rockosi, C., Newberg, H. J., et al. 2009, *AJ*, 137, 4377
- York, D. G., Adelman, J., Anderson, Jr., J. E., et al. 2000, *AJ*, 120, 1579
- Yu, Q., & Tremaine, S. 2003, *ApJ*, 599, 1129
- Yuan, H.-B., Liu, X.-W., Huo, Z.-Y., et al. 2015, *MNRAS*, 448, 855
- Zhang, F., Lu, Y., & Yu, Q. 2010, *ApJ*, 722, 1744
- Zhang, Y.-Y., Carlin, J. L., Yang, F., et al. 2012, *RAA (Research in Astronomy and Astrophysics)*, 12, 792
- Zhang, F., Lu, Y., & Yu, Q. 2013, *ApJ*, 768, 153
- Zhao, G., Zhao, Y.-H., Chu, Y.-Q., Jing, Y.-P., & Deng, L.-C. 2012, *RAA (Research in Astronomy and Astrophysics)*, 12, 723
- Zheng, Z., Carlin, J. L., Beers, T. C., et al. 2014, *ApJ*, 785, L23
- Zhong, J., Chen, L., Liu, C., et al. 2014, *ApJ*, 789, L2